

Electronic Supporting Information

NIR-II Light-Modulated Injectable Self-Healing Hydrogel for Synergistic Photothermal/Chemodynamic/Chemo-therapy of Melanoma and Wound Healing Promotion

Xiaohua Huang,^a Lei Tang,^a Lin Xu,^a Yu Zhang,^a Guangyao Li,^a Weiling Peng,^a
Xiaolu Guo,^{b*} Li Zhou,^a Chanjuan Liu^{a*} and Xing-Can Shen^b

^a. Guangxi Key Laboratory of Optical and Electronic Materials and Devices,
College of Materials Science and Engineering, Guilin University of Technology,
Guilin 541004, China.

^b. State Key Laboratory for Chemistry and Molecular Engineering of Medicinal
Resources, School of Chemistry and Pharmaceutical Science, Guangxi Normal
University, Guilin, 541001, China.

Keywords: Injectable self-healing hydrogel; Iron ion-doped polyaniline; NIR-II
responsive photothermal therapy; Antibacterial infection; Wound healing
acceleration

Part of experimental section:

Reagents and Materials: Aniline, ammonium persulphate (APS), Iron (III) chloride anhydrous (FeCl_3), Borax ($\text{Na}_2\text{B}_4\text{O}_7 \cdot 10\text{H}_2\text{O}$), 3,3',5,5'-Tetramethylbenzidine (TMB) and 1,10-phenanthroline were obtained from Aladdin Reagent Company (Shanghai, China). Guar gum was purchased from Qingzhou Rongmeier Biotechnology Co., Ltd. Cis-diamminedichloroplatinum (II) (CDDP) was obtained from Shanghai Macklin Biochemical Co., Ltd. All solvents and reagents were analytical grade and used as received without further purification. Deionized water was purified by a Millipore system.

Fetal bovine serum (FBS), trypsin, and high glucose Dulbecco's modified Eagle's medium (DMEM) medium were purchased from Gibco (New York, USA). Penicillin-Streptomycin, propidium iodide (PI)/Calcein-AM Assay Kit, 2',7'-dichlorofluorescein diacetate (DCFH-DA) reactive oxygen Assay Kit, and 3-(4,5-dimethylthiazol-2-yl)-2,5-diphenyltetrazolium bromide (MTT) was obtained from Beyotime Biotechnology Co., Ltd. L929 and B16 cell lines purchased from Kunming Cell Bank of CAS (Kunming, China).

General characterization: Fourier transform infrared spectroscopy (FTIR) was performed on a FT-IR spectrometer (Thermo Nicolet Nexus 470, USA) using KBr pellet method at range of 4000 to 400 cm^{-1} . Ultraviolet-visible-near-infrared (UV-Vis-NIR) absorption spectra ranging from 250-1400 nm were collected by PE Lambda 750 spectrophotometer. Thermogravimetric analysis (TGA) was performed by TGA Q500 under nitrogen conditions from ambient temperature to

800 °C with a slope of 10 °C min⁻¹. The hydrodynamic size distribution and zeta potential value were determined by dynamic light scattering (DLS, Malvern Zetasizer Nano-ZS 90). Atomic force microscopy (AFM) images were taken using a Multimode Nanoscope V scanning probe microscopy system (Bruker, Dimension Icon, USA) in the tapping mode. The AFM specimens of GG@PANI(Fe) composites were prepared by dropping dilute GG@PANI(Fe) aqueous dispersed solution on fresh mica substrates and drying at room temperature under nitrogen flow. Morphologies of the freeze-dried hydrogel samples sputtered with gold were observed by scanning electron microscope (SEM) on a JSM-6380LV tungsten filament SEM. The high-angle annular dark-field scanning transmission electron microscopy (HAADF-STEM), elemental mappings, and energy dispersive spectroscopy (EDS) of GG@PANI(Fe) composite were performed on a JEM-2100 transmission electron microscopy (TEM, Japan) at an accelerating voltage of 200 kV. X-ray photoelectron spectrometer (XPS) analysis was acquired on an ESCALAB 250Xi XPS (Thermo Fisher Scientific Inc., Waltham, MA, USA). Rheological tests were carried out on an TA AR1500EX rotational rheometer using a 25 mm parallel plate with a fixed gap of 0.8 mm.

***In vitro* release of CDDP:** The CDDP-loaded hydrogel (denoted as CDDP/GG@PANI(Fe)-borax hydrogel) was prepared by dissolving the CDDP (2.5 mg mL⁻¹) into 1 mL of GG@PANI(Fe) aqueous dispersed solution (concentration of GG@PANI(Fe): 10 mg mL⁻¹), followed by adding with 30 µL

of borax (concentration: 10 mg mL⁻¹) as the crosslinking agents to form a homogeneous precursor solution. After allowing complete gelation, the hydrogels formed and the drug was encapsulated into the hydrogels *in situ*. The CDDP loading efficiency (LE) was estimated to be 0.25% using following equation: LE (%) = (loading amount of drug in hydrogel/total mass of the hydrogel) × 100. The CDDP-laden hydrogel (CDDP/GG@PANI(Fe)-borax) in a dialysate bag was immersed into 3 mL of phosphate balanced solution (PBS) (pH = 6.5 and 7.4) and shaken at a rate of 60 strokes per minute. After that, 3 mL of released medium were regularly taken out and equal fresh PBS buffer was supplemented. For evaluating the on-demand release of CDDP, the drug-laded CDDP/GG@PANI(Fe)-borax hydrogel was exposed under 1064 nm laser for 10 minutes each time (0.5 W cm⁻²). 3 cycles of laser on (10 minutes) and off (10 minutes) processes were performed. The concentration of CDDP in the release medium was measured by using an inductive coupled plasma optical emission spectrometer (ICP-OES, PerkinElmer Ltd, USA).

***In vitro* biocompatibility evaluation:** The cytotoxicity and hemolysis were used for biocompatibility assay of the obtained hydrogel in this work. L929 cells (mouse fibroblasts) were utilized to evaluated the cytocompatibility of the as-prepared hydrogel. The cells were seeded in 96-well plates at 1.0 × 10⁴ cells per well seeding density, and incubated for 24 h in DMEM media containing 10% FBS, 1% penicillin-streptomycin at 37 °C (5% CO₂). Next, the culture medium in each well was replaced by 200 μL fresh medium, and the sterilized hydrogel

including GG-borax, GG@PANI-borax, and GG@PANI(Fe)-borax were respectively added into the well plate, the culture medium and hydrogels were removed after co-incubated with the cells for another 12 h, and the relative cell viability was determined by the standard MTT assay. The cells co-cultured with DMEM alone were used as the negative control group. The resultant absorbance values at 570 nm of the medium were acquired by a microplate reader. *Cell viability* = $(A_t / A_0) \times 100\%$, Where A_t is the absorbance of experiment groups, A_0 represent the absorbance of the control group. Furthermore, to visually detect the cellular survival, the Live/dead stained assay was performed *via* co-staining the treated L929 cells with Calcein AM and PI. Finally, it was observed using a fluorescence microscope (Olympus, CKX53).

For hemolysis assays, 2.5 mL fresh whole blood was collected from healthy Kunming mice, then centrifuged to obtain the red blood cells (RBC). Next, 2% RBC suspended in physiological saline was added with GG-borax, GG@PANI-borax and GG@PANI(Fe)-borax. Distilled water was used as a positive control and PBS buffer was used as a negative control. After incubated at 37 °C for 2 h, following centrifuged at 3000 rpm for 5 minutes, the absorbance value of the supernatant at 576 nm was recorded. The calculation formula of hemolysis rate is as flows: *Hemolysis rate (100%)* = $(A_{sample} - A_{negative}) / (A_{positive} - A_{negative}) \times 100\%$. Where A_{sample} is the absorbance of experimental group, $A_{negative}$ is the absorbance of negative control, and $A_{positive}$ is the absorbance of positive control.

***In vitro* Intracellular •OH detection:** Intracellular •OH generation was detected

using the DCFH-DA Assay Kit. B16 cells (1.0×10^4 cells/well) were seeded in 48-well plates and incubated for 24 h in advance. The cells were then cultured for another 6 h under different conditions: Blank, H_2O_2 , GG@PANI(Fe)-borax, GG@PANI(Fe)-borax + H_2O_2 + pH 7.4, and GG@PANI(Fe)-borax + H_2O_2 + pH 6.5 (with or without 1064 nm laser irradiation for 2 minutes), the concentration of hydrogel and H_2O_2 were $400 \mu\text{g mL}^{-1}$ and 1 mM, respectively. Following by removing the gel and medium, then rinsing the cells with PBS for three times, the indicator solution (DCFH-DA) was added according to the standard protocol. After incubation for additional 20 minutes, PBS was used to rinsed the excessive indicator, and fluorescence images of the treated cells were acquired by a fluorescence microscope.

Antibacterial activity evaluations *in vitro*: The antimicrobial activities of the as-prepared hydrogels were assessed against *Escherichia coli* (*E. coli*, ATCC 25922) and *Staphylococcus aureus* (*S. aureus*, ATCC 12605). For the colony formation assays, 1 mL of bacterial suspension in Luria-Bertani (LB) broth (1.5×10^6 CFU mL^{-1}) was added to small glass vials containing GG-borax, GG@PANI-borax and GG@PANI(Fe)-borax, respectively. The bacterial suspension untreated with hydrogels was used as control. After co-incubation at 37 °C for 2 h in an incubator, the bacterial suspensions in each group (100 μL) were spread on the corresponding solid LB agar culture dishes. The colonies were formed after 24 h of incubation at 37 °C. Subsequently, the colony-forming units (CFU) on each LB agar plate were recorded by a camera. Each group was tested

in triplicate and the antibacterial ratio was determined as follows: antibacterial ratio (%) = (colony number of control - colony number of hydrogel)/colony number of control \times 100%.

Statistical Analysis: All of the quantitative data were expressed as mean \pm standard deviation (SD). The statistical analysis between groups was analyzed by SPSS using one-way analysis of variance (ANOVA). The probability value (P-value) less than 0.05 was considered to be statistically significant.

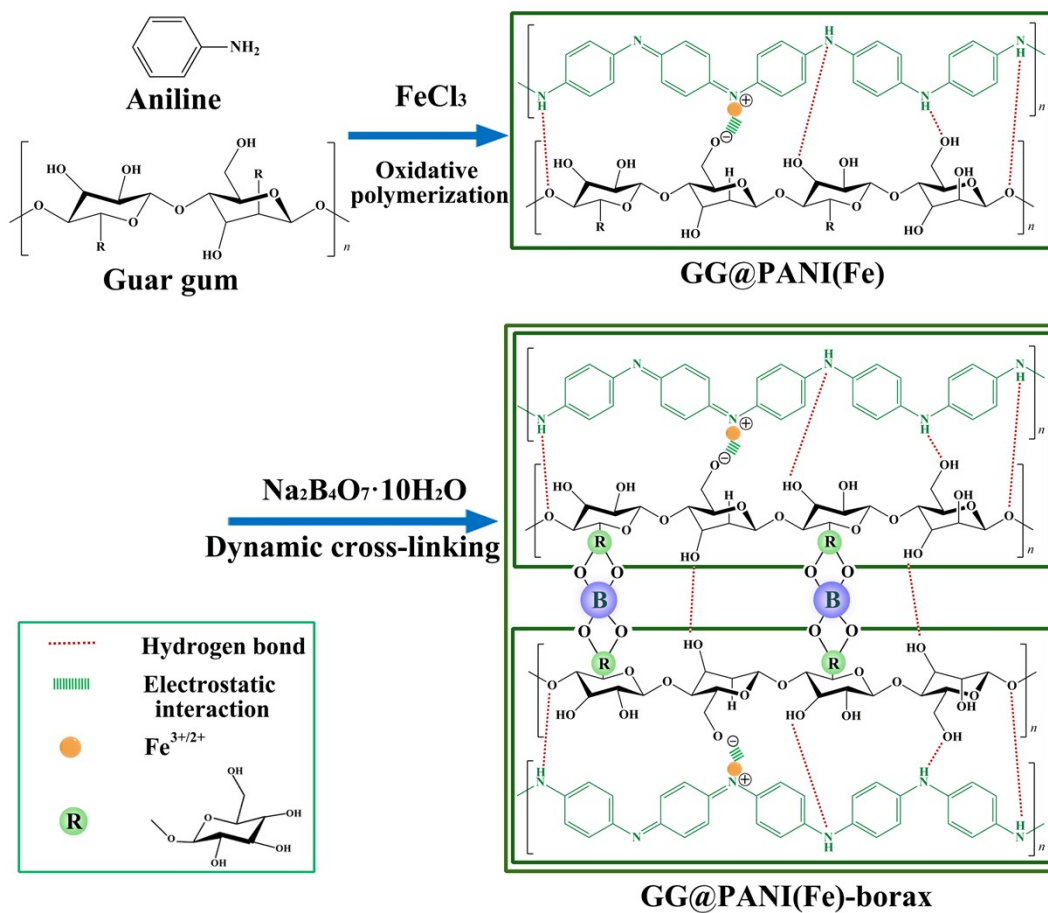


Figure S1. Schematic illustration of the preparation process of GG@PANI(Fe)-borax.

Table S1. Size (z-average particle diameter $D_z \pm SD$), polydispersity index (PDI $\pm SD$) and zeta potential of GG@PANI(Fe) composites prepared by the oxidation of aniline with $FeCl_3$ in the presence of GG with varying GG/ANI feed weight proportion.

GG:ANI ^a	As-prepared			After seven days		
	Size (nm)	PDI	Zeta potential (mv)	Size (nm)	PDI	Zeta potential (mv)
0:1	95 ± 2.94	0.10 ± 0.007	+ 24.5 ± 0.52	Precipitate formation		
0.5:1	123 ± 6.53	0.12 ± 0.008	+ 13.9 ± 0.32	132 ± 6.16	0.30 ± 0.011	+ 11.9 ± 0.72
1.05:1	173 ± 5.79	0.11 ± 0.009	+ 6.8 ± 0.85	182 ± 8.73	0.26 ± 0.009	+7.1 ± 0.53
1.5:1	485 ± 8.61	0.26 ± 0.010	- 1.99 ± 0.43	481 ± 10.2	0.34 ± 0.011	-1.58 ± 0.14

^a GG/ANI feed weight proportion during the preparation of GG@PANI(Fe) composites.

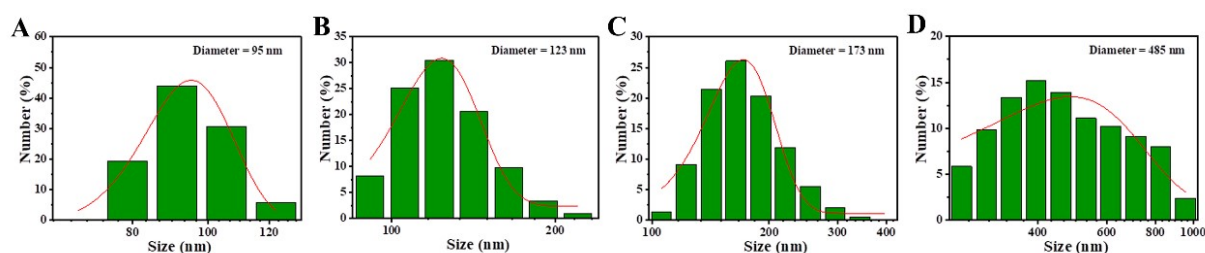


Figure S2 Size distribution of prepared GG@PANI(Fe) composites under varying feed ratio of GG/ANI 0:1 (A), 0.5:1 (B), 1.05:1 (C), and 1.5:1 (D).

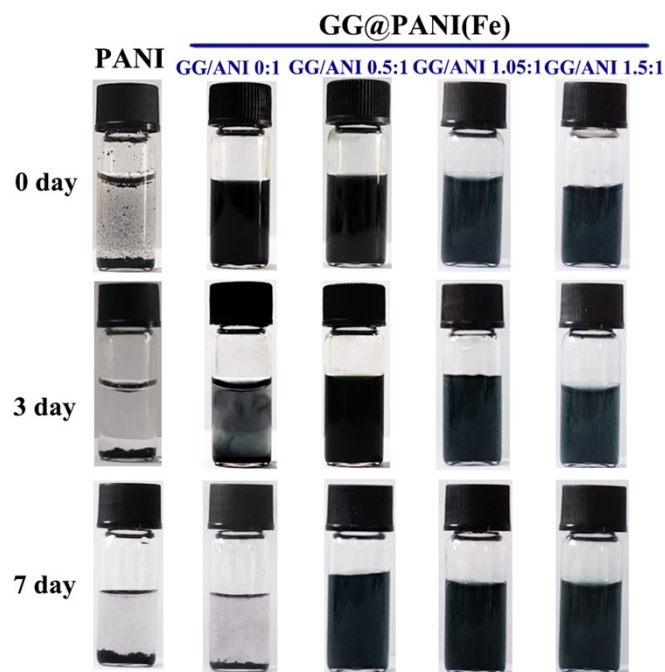


Figure S3 Stability photographs of PANI and GG@PANI(Fe) composites (prepared under varying feed ratio of GG/ANI) in water.

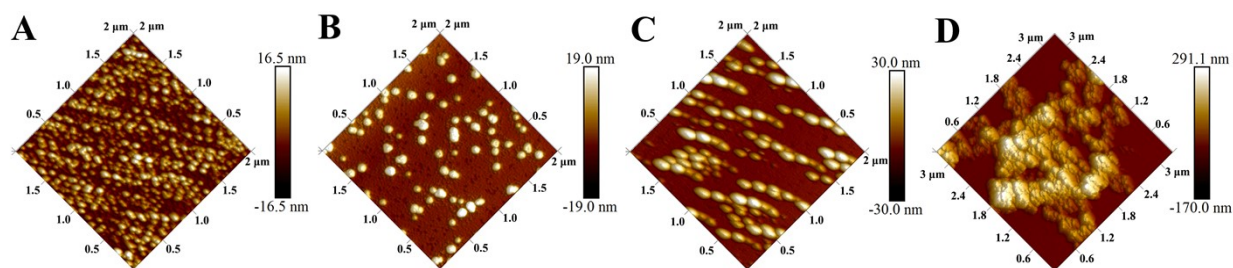


Figure S4 AFM images of GG@PANI(Fe) composites synthesized with GG/ANI feed weight ratio of 0:1 (A), 0.5:1 (B), 1.05:1 (C), and 1.5:1 (D).

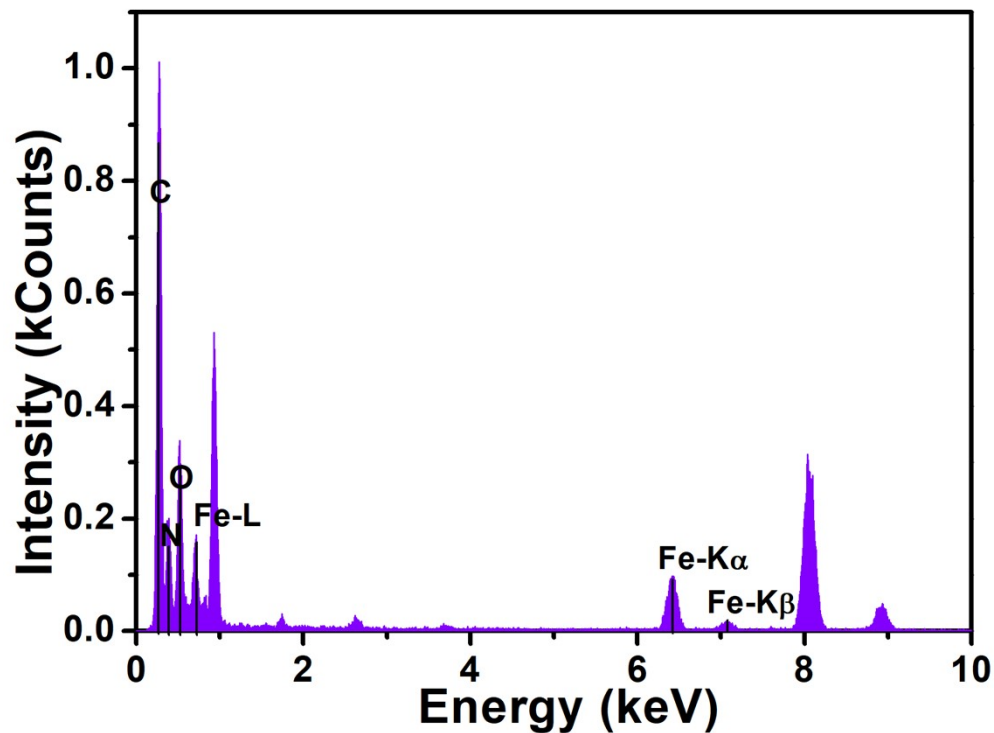


Figure S5 EDS analysis for GG@PANI(Fe) composite.

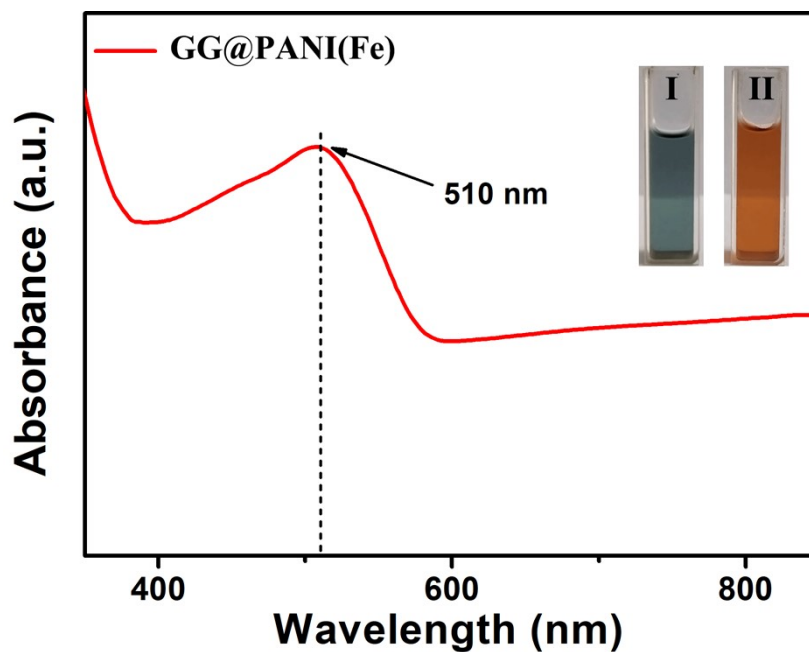


Figure S6 UV-vis absorption of GG@PANI(Fe) composite after reaction with 1,10-phenanthroline, the inset shows the supernatant (I: GG@PANI(Fe); II: GG@PANI(Fe) + 1,10-phenanthroline).

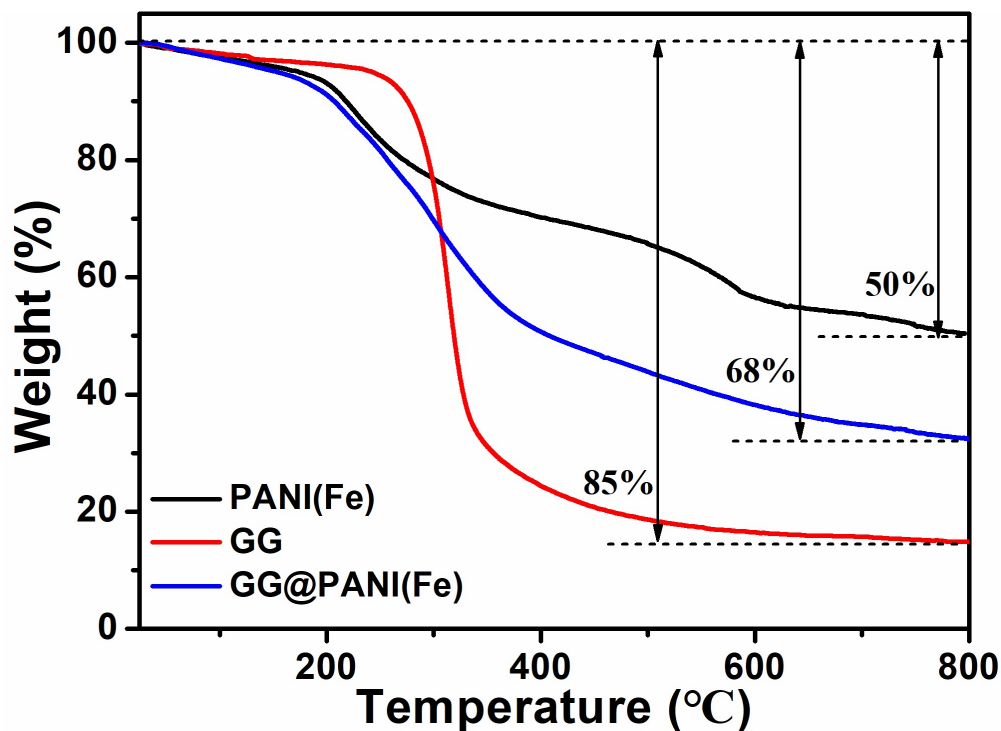


Figure S7 TGA curves of PANI(Fe), GG and GG@PANI(Fe). It was obviously noted that the PANI(Fe) had good thermal stability (with 50% weight loss at 800 °C) because of the rigid aromatic ring, while the flexible GG chain showed lower thermal performance (with 85% weight loss at 800 °C). And the heat-resistant performance of GG@PANI(Fe) composite was between original PANI(Fe) and GG (with 68% weight loss at 800 °C). The ratio of PANI(Fe) and GG was estimated based on the formula below.

$$0.50x + 0.85y = 0.68 \dots\dots\dots (1)$$

$$x + y = 1 \dots\dots\dots (2)$$

x and y are weight percentage of PANI(Fe) and GG, respectively. The content is determined to be 51% for GG and 49% for PANI(Fe), respectively.

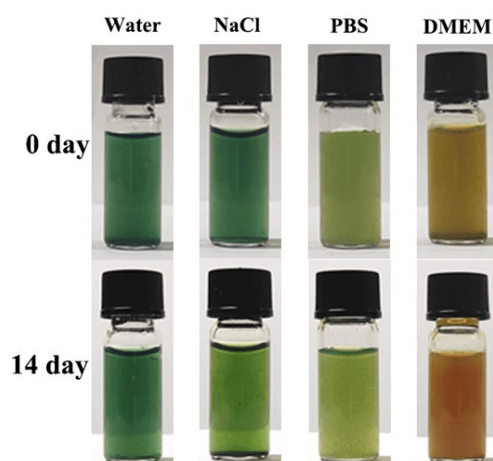


Figure S8 Stability of GG@PANI(Fe) composite in different solutions (including deionized water, 0.9% NaCl, PBS and DMEM medium).

Table S2. Preparation of GG@PANI(Fe)-borax hydrogel.

GG:ANI ^a	GG@PANI(Fe)	borax	Gelation time	Gel Stability in PBS
0.5:1			> 24 h	~ 2 h
1.05:1	10 mg/mL	0.3 mg/mL	1.88 min	> 14 days
1.5:1			0.42 min	> 14 days

^a GG/ANI feed weight proportion during the preparation of GG@PANI(Fe) composites.

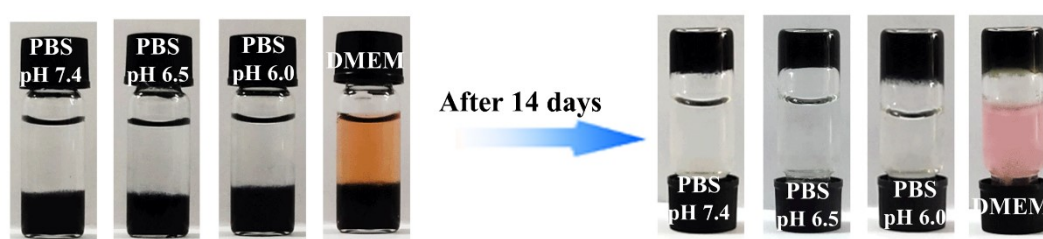


Figure S9 Stability of GG@PANI(Fe)-borax hydrogel (the GG@PANI(Fe) prepared with the GG/ANI feed ratio of 1.05:1) in different solutions (including DMEM medium and PBS with different pH values, measured at ambient temperature).

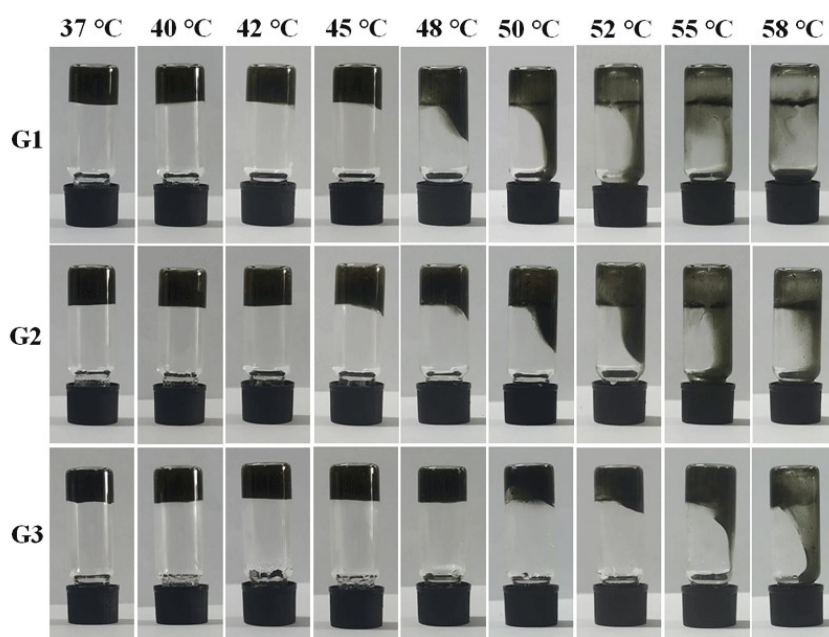


Figure S10 Digital photographs of Gel-sol transition process for G1, G2, and G3, (G1, G2, and G3 were prepared by mixed solution of 0.3 mg/mL borax and 10 mg/mL, 15 mg/mL and 20 mg/mL GG@PANI(Fe) composites, respectively, of which GG@PANI(Fe) was synthesized under GG/ANI feed ratio of 1.05:1). As the temperature increased, the hydrogels gradually melted into sol and flowed down, the melting temperatures of G1, G2, and G3 were 48, 50 and 55 °C, respectively.

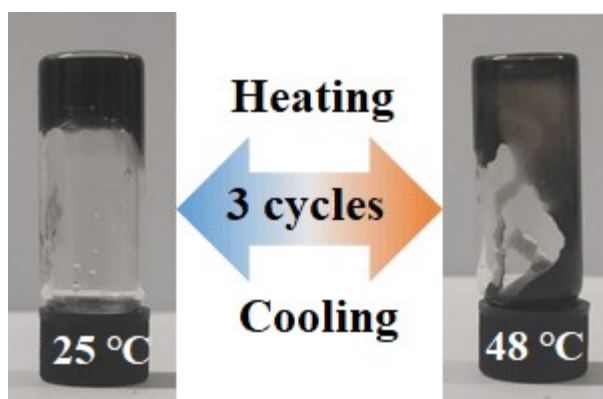


Figure S11 The thermo-sensitive and reversible gel-sol transition of the GG@PANI(Fe)-borax (G1). The hydrogel underwent a gel-sol transition when the

temperature was over 48 °C, and the converted sol gradually recovered to gel phase again during the cooling period even after 3 cycles.

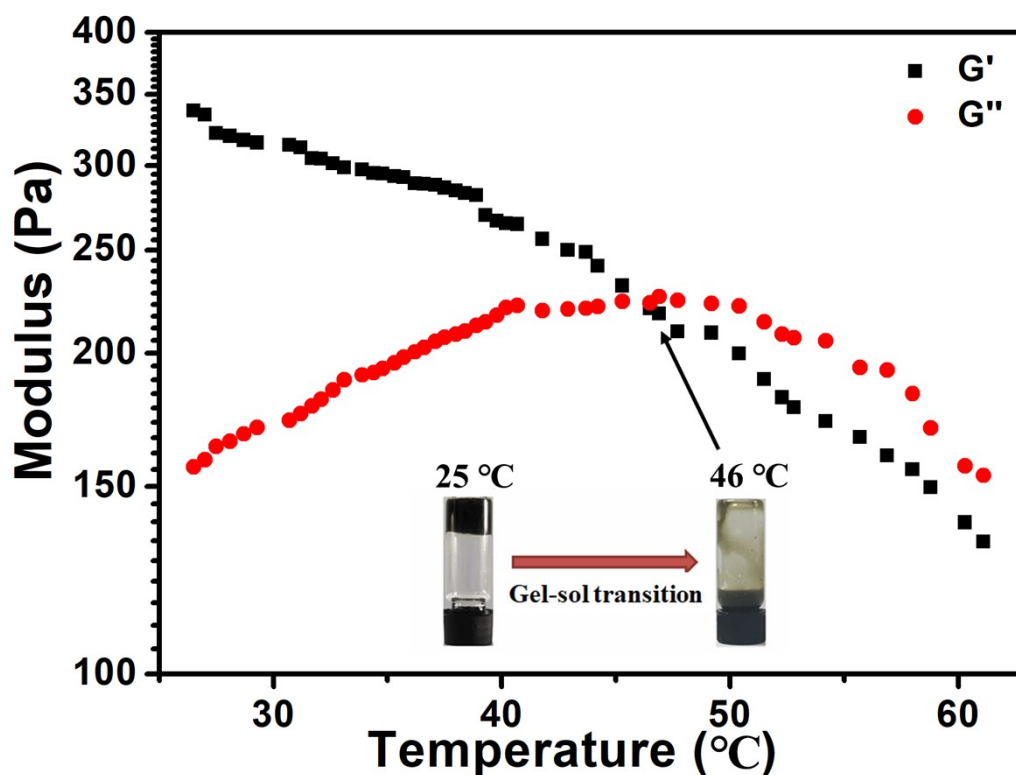


Figure S12 The temperature-dependent evolution of G' and G'' modulus for GG@PANI(Fe)-borax (G1).

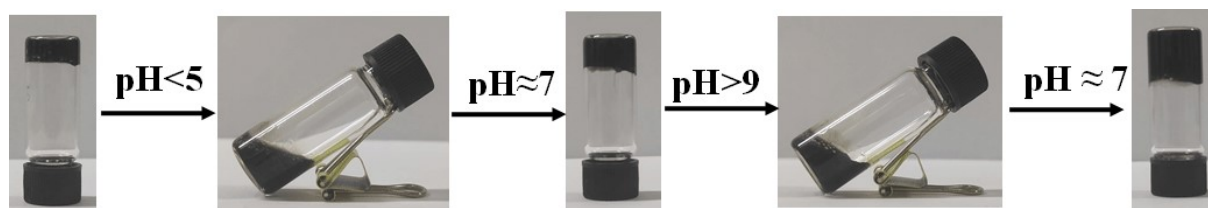


Figure S13 The reversible pH-responsive gel-sol transition of GG@PANI(Fe)-borax hydrogel. GG@PANI(Fe)-borax hydrogel underwent a gel-sol transition at $\text{pH} < 5$ and $\text{pH} > 9$, and gradually recovered to gel phase when the pH value was approximately 7.

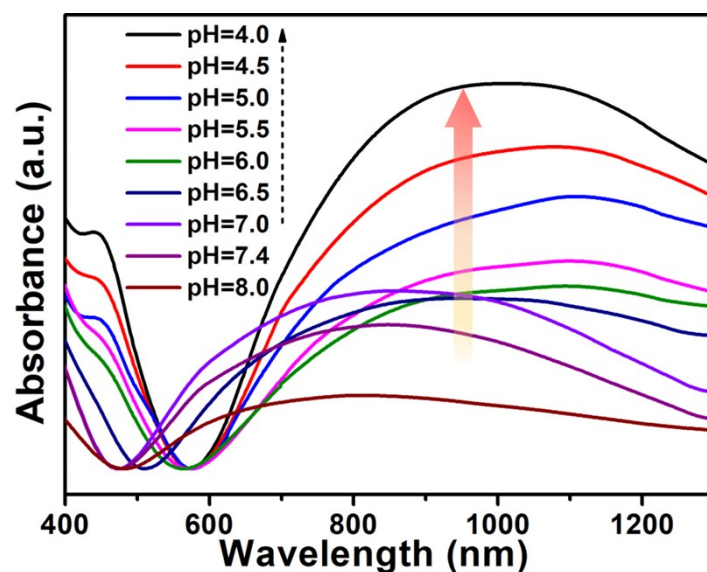


Figure S14 UV-vis-NIR spectra of GG@PANI(Fe)-borax precursor in different pH buffer.

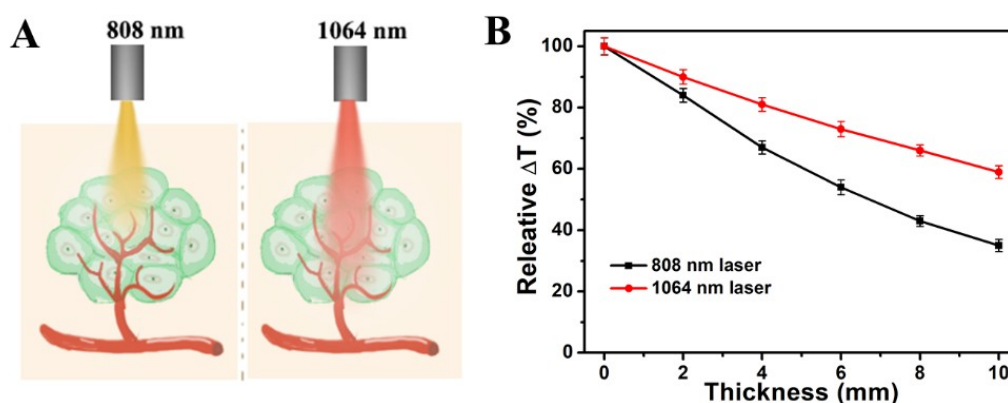


Figure S15 (A) Scheme that illustrates the deeper tissue penetration of 1064 nm relative to that of 808 nm. (B) Normalized temperature elevations of GG@PANI(Fe)-borax hydrogel exposed to tissue-penetrating lasers (1064 and 808 nm laser at the power density of 0.5 W cm^{-2} , respectively).

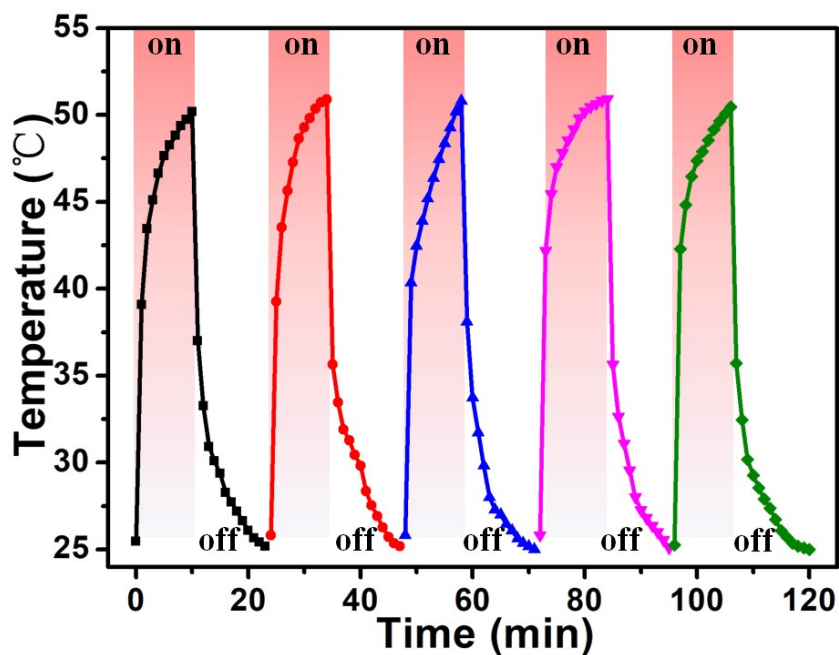


Figure S16 Temperature profiles of GG@PANI(Fe)-borax hydrogel for five successive cycles of 808 nm laser on (10 min, 0.5 W cm^{-2}) and off processes.

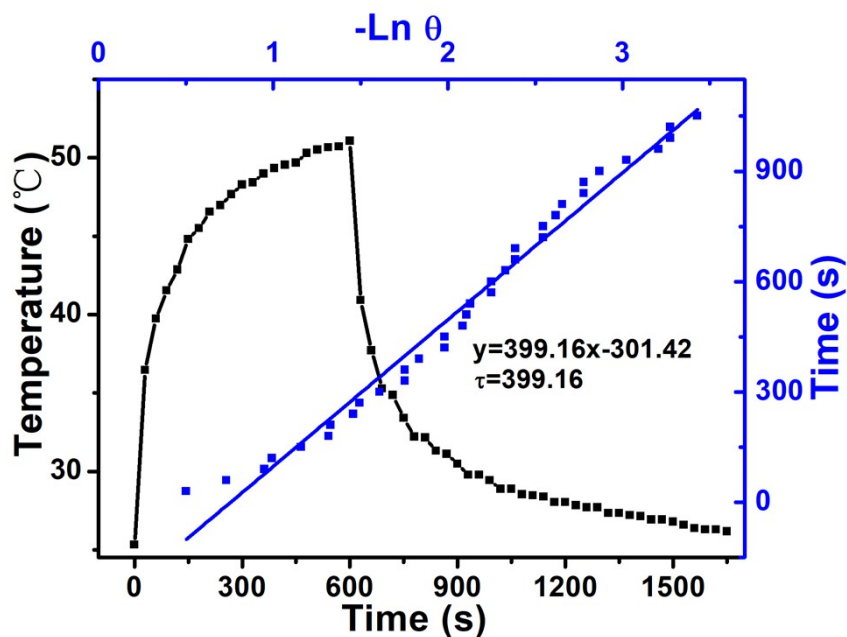


Figure S17 Calculation of the photothermal conversion efficiency. Black line: photothermal heating curve of GG@PANI(Fe)-borax hydrogel under the irradiation with 1064 nm laser (0.5 W cm^{-2}) for 10 min, and the cooling curve after the laser was switched off. Blue line: linear time data versus $-\ln\theta$ obtain from

the cooling period. Time constant (τ) for the heat transfer was determined by applying the linear time data from the cooling period. The photothermal conversion efficiency (η) was calculated according to the following equations:

$$\eta = \frac{hA\Delta T_{max} - Q_s}{I(1 - 10^{-A_\lambda})}$$

h was heat-transfer coefficient, A was the surface area of the sample container, ΔT_{max} was the maximum temperature change ($\Delta T_{max} = T_{max} - T_{surr}$, T_{max} was the equilibrium temperature; T_{surr} was surrounding temperature). Q_s was the heat associated with the light absorbance of the solvent (pure water). I was the laser power density. A_λ was the absorbance value at 1064 nm. θ is defined as the ratio of ΔT and ΔT_{max} , the introduction of which can get the value of hA :

$$\theta = \frac{\Delta T}{\Delta T_{max}}$$

ΔT was defined as $T - T_{surr}$ (T and T_{surr} are the sample temperature and ambient temperature, respectively). Therefore, hA can be determined as following:

$$hA = \frac{mC_p}{\tau}$$

τ was the slope $v_s - \ln\theta$ of linear time data from the cooling period. m and C_p were the mass and heat capacity of water, respectively.

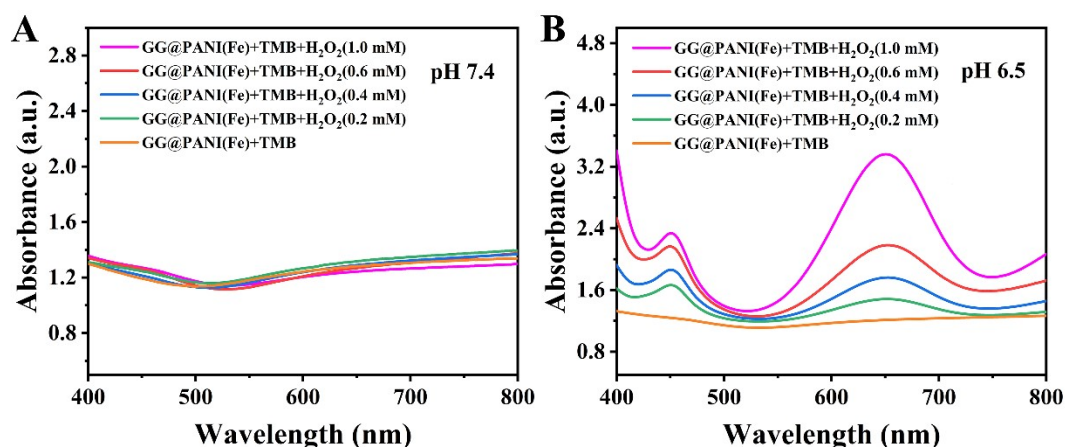


Figure S18 The UV-vis absorption spectra of GG@PANI(Fe) + TMB upon the addition of elevated concentrations of H₂O₂ at pH 7.4 (A) and pH 6.5 (B).

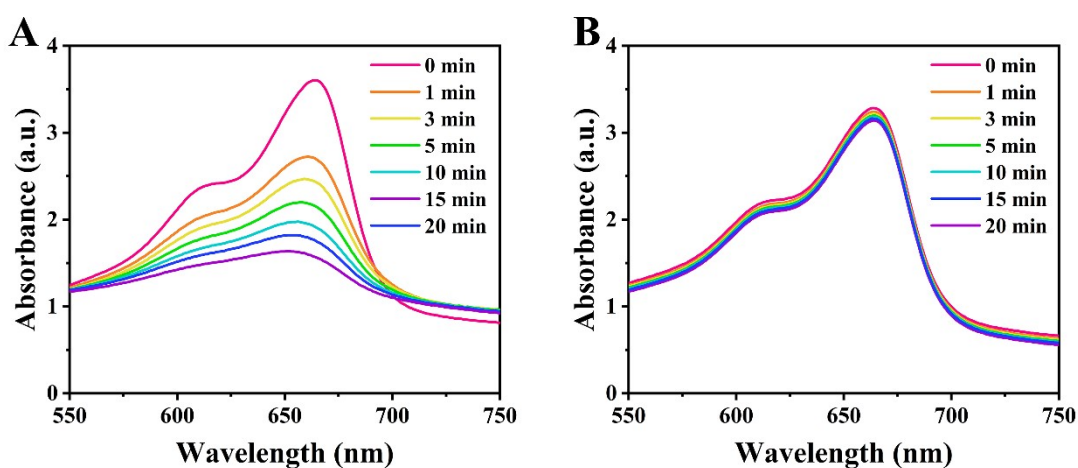


Figure S19 (A) the UV-vis absorption spectra of MB treated with GG@PANI(Fe)-borax (precursor) and H₂O₂ (0.8 mM) solution at pH 6.5. (B) the UV-vis absorption spectra of MB treated with GG@PANI(Fe)-borax (precursor), H₂O₂ (0.8 mM) and DMSO (50 μ L) solution at pH 6.5.

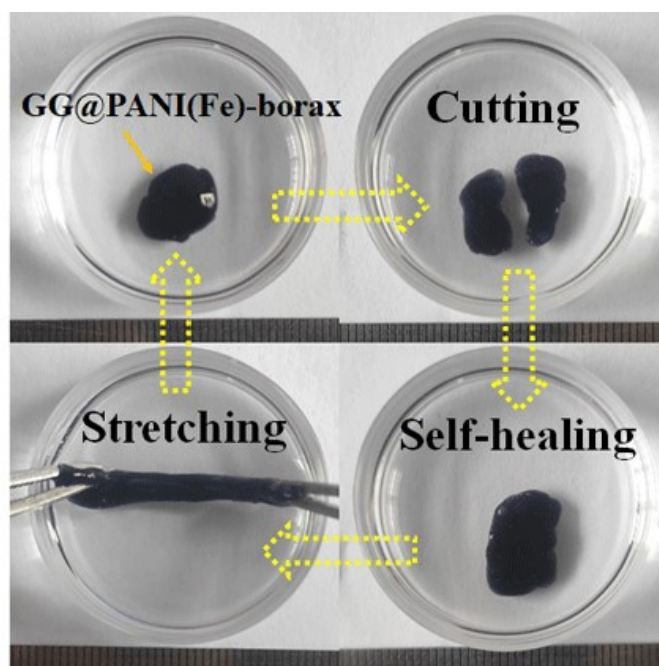


Figure S20 Self-healing behavior of GG@PANI(Fe)-broax under PBS buffer. A piece of hydrogel was immersed in PBS buffer and then it was cutted into two halves, which can combined into a single piece again when they were put together, and the self-healing gel could be strethced up to certain lenth without breaking.

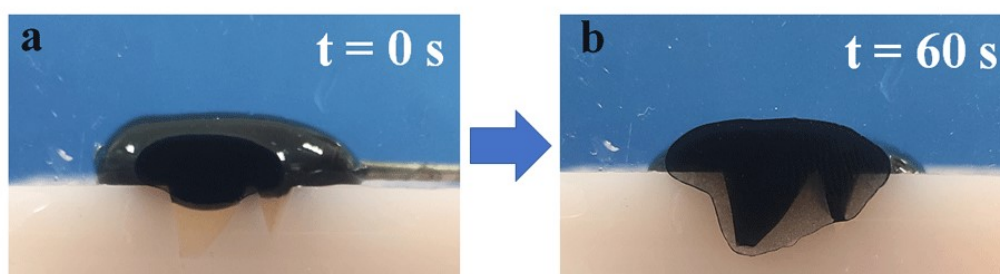


Figure S21 Self-adaptive performance of GG@PANI(Fe)-borax. (a) A piece of hydrogel was covered on the irregular notches of a plastic mold, (b) the irregular notches were completely filled with hydrogel without external force after 60 s, indicating the excellent and rapid self-adaption ability.

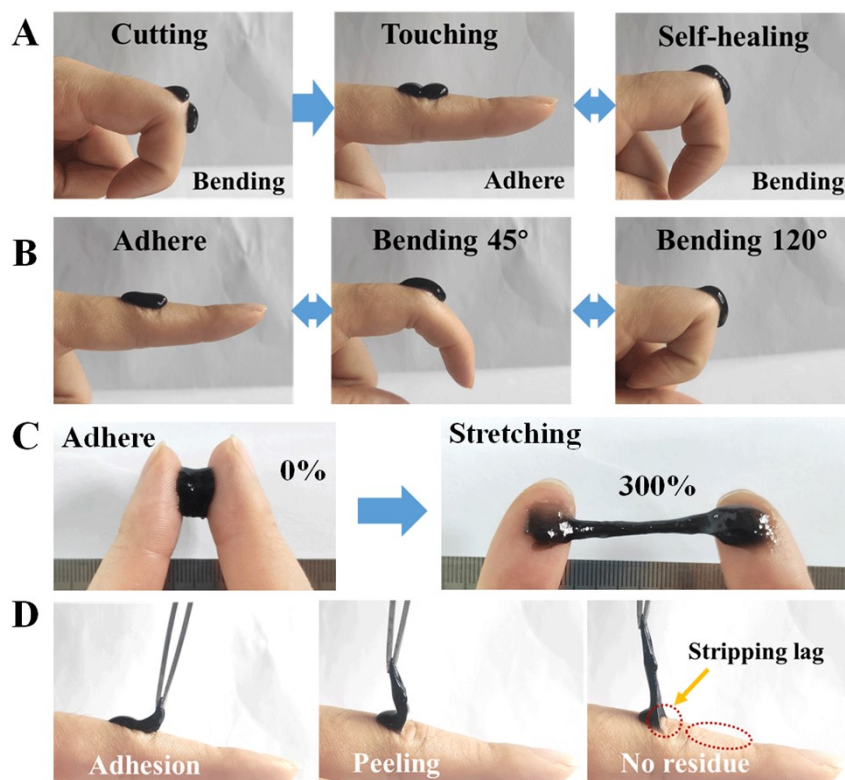


Figure S22 The GG@PANI(Fe)-borax hydrogel tightly adhered to the finger skin and accommodated its movements without shedding off after bending into different angles or even stretched to 300%, and there is no residue after being peeled off from skin.

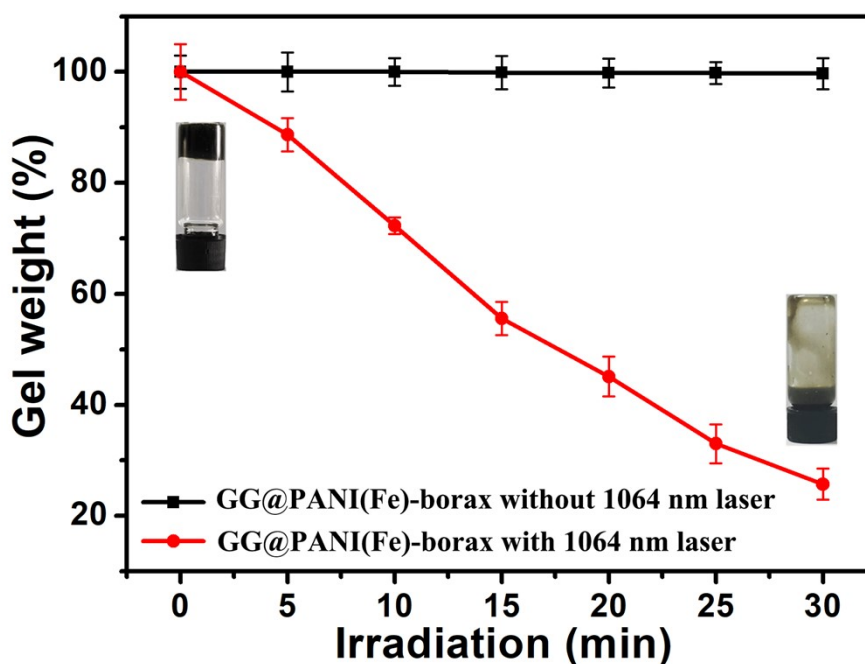


Figure S23 NIR-triggered gel-sol conversion of GG@PANI(Fe)-borax hydrogel under a 1064 nm laser (0.5 W cm^{-2}) irradiation, the illustrations shows the gel-sol transition image.

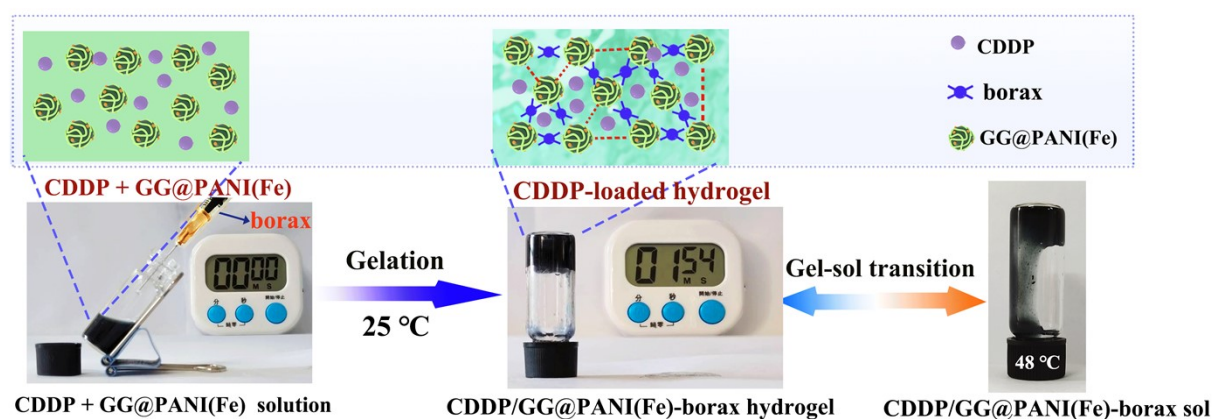


Figure S24 Preparation process and thermosensitive gel-sol transition photographs of CDDP-loaded hydrogel (CDDP/GG@PANI(Fe)-borax). The addition of CDDP has negligible effect on gelation time and gel-sol transition temperature.

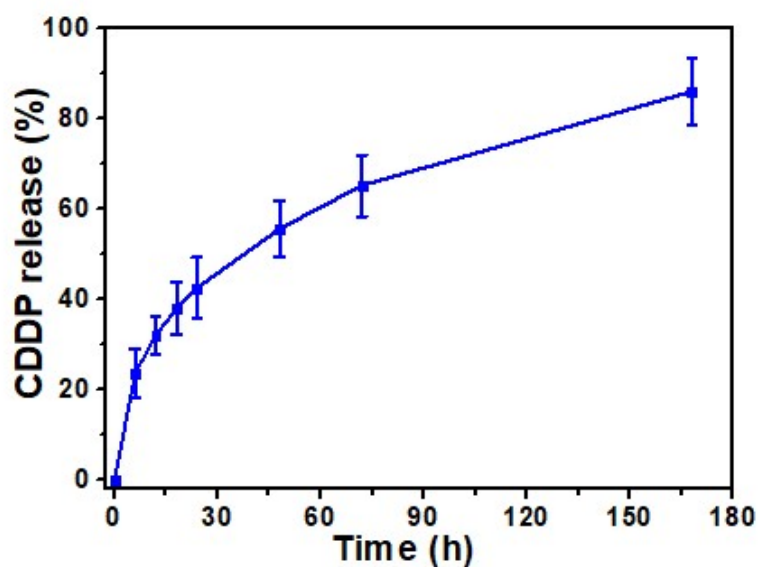


Figure S25 Long-term release of CDDP from the GG@PANI(Fe)-borax hydrogel in PBS solution without laser irradiation.

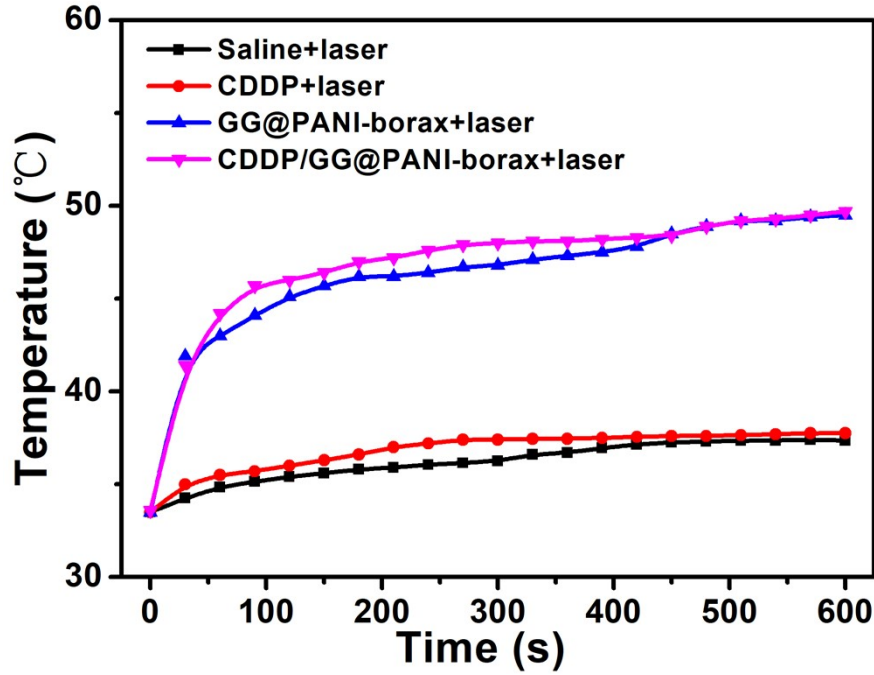


Figure S26 The irradiated area temperature profiles of B16 tumor-bearing mice after different treatment and following exposure to a 1064 nm laser (0.15 W cm^{-2} , 10 minutes) taken at the first day.

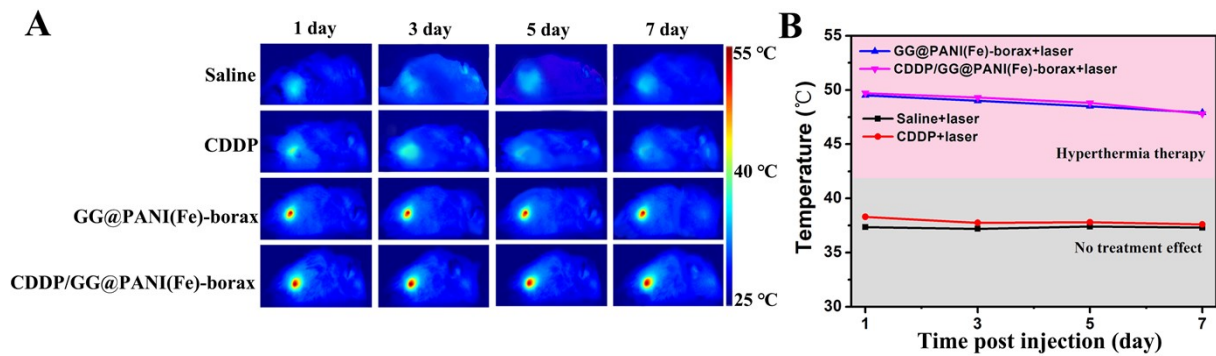


Figure S27 (A) Infrared thermal images of B16 tumor-bearing mice after 10 min of treatment with a 1064 nm laser (0.15 W cm^{-2}) during four laser treatments, (B) the corresponding maximum temperature profiles of the irradiated area.

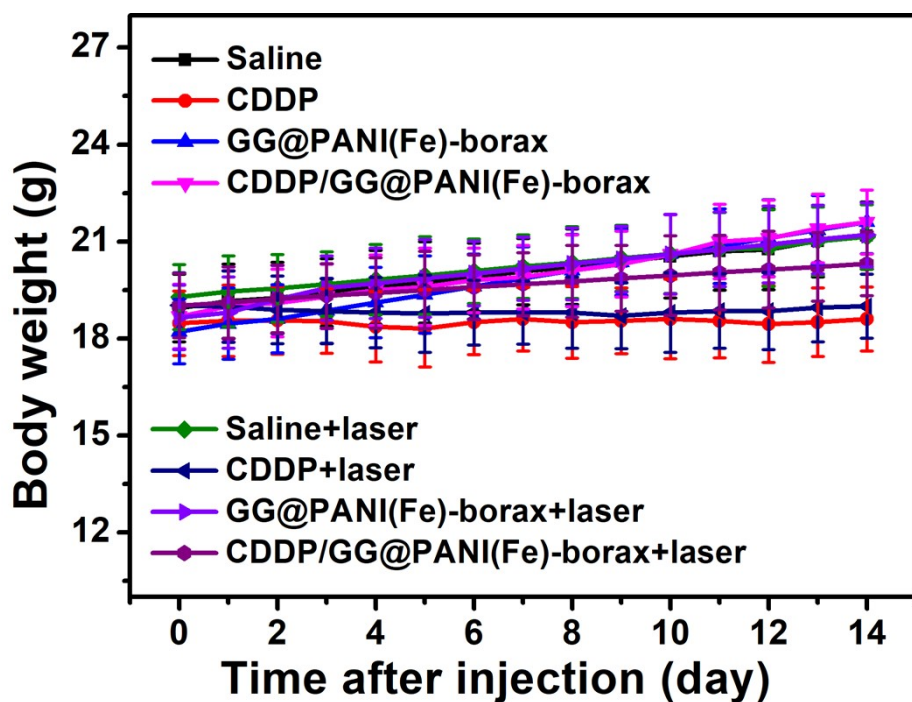


Figure S28 Body weight curves of different groups during treatment.

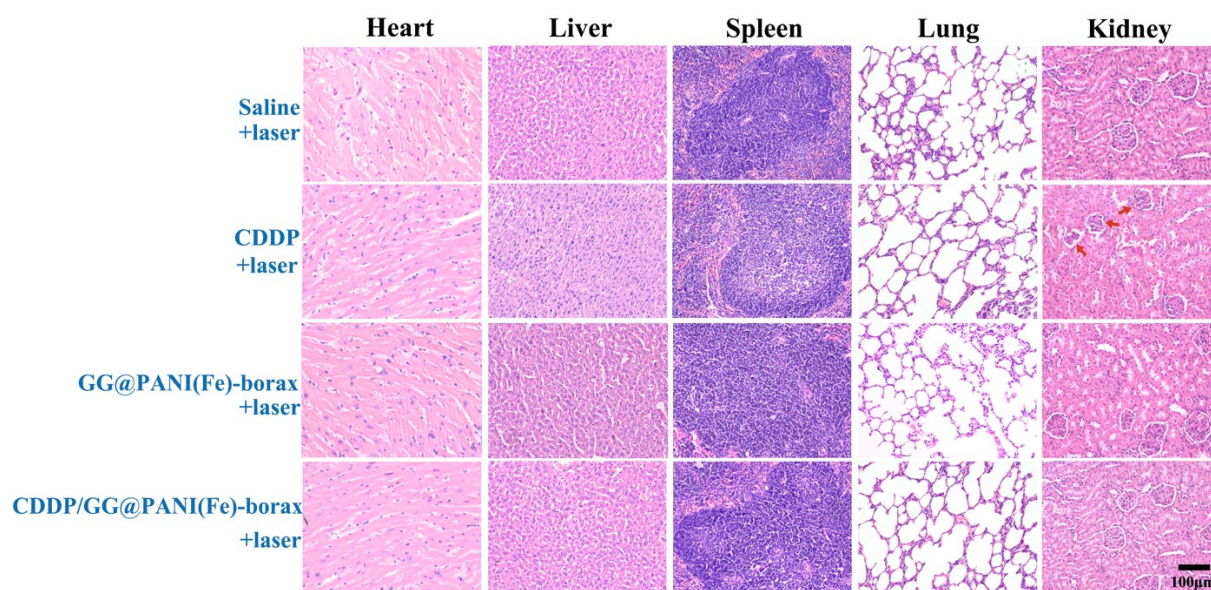


Figure S29 H&E staining of the major organs (including heart, liver, spleen, lung and kidney) harvested from the mice after treatment. In the H&E staining, the nuclei were stained bluish violet, and the cytoplasm and extracellular matrix were stained pink. For free CDDP group, the slightly nephrotoxicity caused by free CDDP. For the CDDP/GG@PANI(Fe)-borax group, all of the major organs

showed no obvious detectable lesions or pathological changes, indicating that GG@PANI(Fe)-borax hydrogel was biocompatible and the toxicity of CDDP can be reduced by encapsulating CDDP into hydrogel.

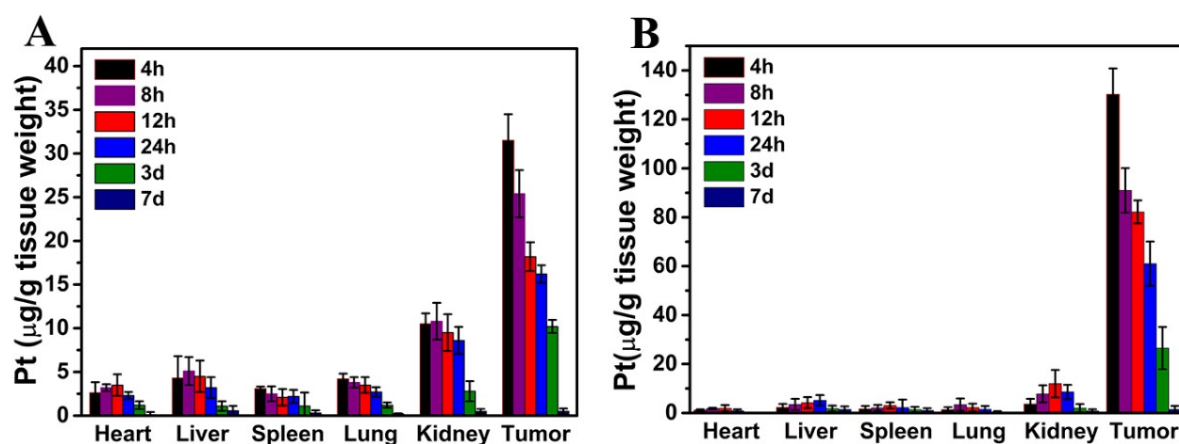


Figure S30 The biodistribution of CDDP in the tumors and the major organs after the intratumoral injection of 100 µL (A) free CDDP (4 mg CDDP/kg body weight) and (B) CDDP/ GG@PANI(Fe)-borax hydrogel (at a doses of 4 mg CDDP/kg body weight). At predetermined time interval (4 hours, 8 hours, 12 hours, 24 hours, 3 days and 7 days) after the injection, the mice were sacrificed and the main organs together with tumors were lyophilized and weighed, then they were digested in aqua regia for 2 h for dissolution of the tissues. After that, the concentrations of Pt were quantified by ICP-MS analysis. Clearly, for the CDDP/GG@PANI(Fe)-borax hydrogel group, the CDDP mainly concentrated at the tumor sites, with less nonspecific distribution to the major organs as compared with the free CDDP groups. This observation confirmed that the GG@PANI(Fe)-borax hydrogel could maintain higher accumulation rate of the CDDP in tumors, effectively avoiding nonspecific distribution of drugs.



Figure S31 Photograph of the GG@PANI(Fe)-borax hydrogel injected into the infected wound.